Magnetic Diagnosis of Iron-based Materials and their Monte-Carlo Simulations

Koji Yamada[1)], Yoshihiro Isobe[2)] and Katsuhiko Yamaguchi[3)]

1) Dept. Functional Materials Science, Saitama University, Saitama 338-8570, Japan
2) Nuclear Fuel Industries Limited, Sennan-gun, Osaka 590-0481, Japan
3) Dept. Physics, Fukushima University, Fukushima 960-1296, Japan

ABSTRACT

Nondestructive evaluations of iron-based materials were investigated for low alloy steels as A533B, S25C and stainless steels as SUS304, SUS316 by a magnetic leakage field sensor of GaAs Hall element, a directionally sensitive pick-up coil of magnetic Barkhausen noises and residual stresses obtained by X-ray diffractions, in applied tensile stress ranges up to their fracture states. An index of a average field for discontinuous magnetizations in materials was derived by normalized magnetic noise amplitude. We found the index linearly reflects the degree of residual strains to some extents in ferromagnetic materials and even in paramagnetic stainless steels via martensitic transformations.

INTRODUCTION

The nondestructive evaluations (NDE) for degradations in iron-based structural materials are very important to protect our modern society because of the gigantic scales in atomic power plants or any other chemical plants. However, NDE are not always performed by experienced engineers with high costs. In this study, we have developed a technology easy for inspectors in factories. This technology mainly consisted in magnetic inspections of leakage flux distribution and magnetic Barkhausen noise observations, respectively. These have the following special features [1,2,3,4,5,6]. The leakage flux distribution of samples was observed to know the material constant inhomogeneity via lattice imperfections and magnetic residual magnetizations at each point. For this purpose, we use a semiconductor Hall element of GaAs as small as 120 μ m square with a very short lift-off distance of 200 μ m from the surface, in contrast to that by SQUID (lift-off distance of about 5mm typical). An intentional sample polarization was performed before the distribution observation to avoid the spurious magnetizations by globe field, other surrounding electrical machines or/and magnetized tools. The distributions of degradations at each position were well visualized by the first derivatives of the normal components of leakage fluxes along applied stresses. The magnetic Barkhausen noises (MBN) of samples were observed with a pick-up coil to detect the amount of discontinuous magnetization at each point, that reflects the local lattice voids via the intensities of magnetic domain pinning forces [7]. The averaged fields ($<H_D>$) at each position for their discontinuous magnetizations were derived as an indicator of the residual stress or degradation by using normalized BMN amplitudes. The parameter $<H_D>$ become insensitive to the touching manner of the pick-up coil at the sample surface with various stains and scratches, and become sensitive to the noise distribution as a function of applied fields up to the saturation magnetization. Further, $<H_D>$ showed a linear relationship with residual stresses in a stress range up to several percents of residual strains for A533B and stainless steels.

By using MBN detections, we attained an enough sensitivity of residual strains as small as 0.2 % for S25C, A533B and 3 % for SUS304, S316, respectively. In the present paper we also tried to simulate magnetizations of a 50x50x50 spin cube with a planar atomic voids by using RKKY model. We obtained a temperature dependence of magnetizations differently with and without atomic voids, respectively [8, 9, 10, 11]. These will be explained in the discussions.

EXPERIMENTAL SETUP AND RESULTS

The samples of S25C, A533B, SUS304 and SUS316 were prepared in typical shapes of 60x165x2^t mm or 60x165x5^t mm as shown in Fig.1 (a) on a plotter bench. These chemical compositions, yields and the annealing conditions are summarized in the appendix. Experiments of magnetic leakage flux observations were performed by using a semiconductor Hall element as mentioned in the introduction and the current in the Hall element was operated by a lock-in-amplifier system with a reference frequency at 10kHz [2]. The samples were magnetically polarized in a saturation field of 80kA/m before measurements, to avoid

any spurious polarizations by e.g. globe field or other surrounding machines. The Hall element was mounted at the pencil position in a plotter with each scanning step of about 50 μ m. We measured the remanent states of the material. Fig.1 shows an example of the leakage flux distribution pattern ($B_Z(x,y)$) of S25C together with the first derivative of $dB_Z(x,y)/dx$, where coordination system is inserted in Fig.2.

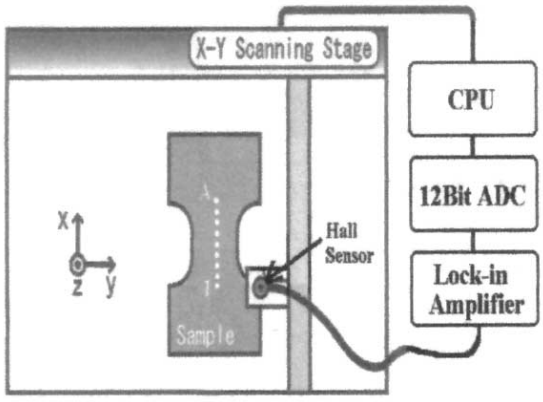

Fig.1 The experimental set-up of the leakage flux observation.

Note 1. The alphabets "A"-"I" in the sample on the plotter denotes the positions for MBN measurements.

Note 2. The measurements were performed after an

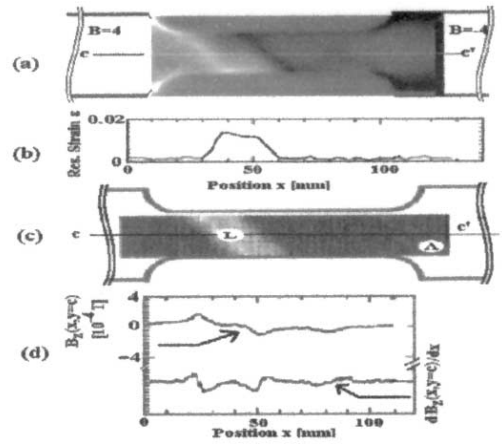

Fig.2. The Typical leakage flux distributions for an A533B sample with a residual strain of 0.38 %.

(a) $B_Z(x,y)$, (b) ε (x,y=c), (c) $dB_Z(x,y)/dx$,

(d) $B_Z(x,y=c)$ and $dB_Z(x,y=c)/dx$

Note:B(-)&W(+) for outwards (+) and inwards (-),

Fig.2 (a) shows the top view of the leakage flux distribution colored in B(-) and W(+), where white color denotes the going out flux from the surface, vice versa. (b) shows the directly observed residual strain by XRD, (c), the first derivative of the distribution along x direction, (d) numerical value of the leakage flux and its first derivative along the sample (c-c'). It must be noted here that the locations of the heavily strained positions are visualized by the first derivative as in (b) and (c).

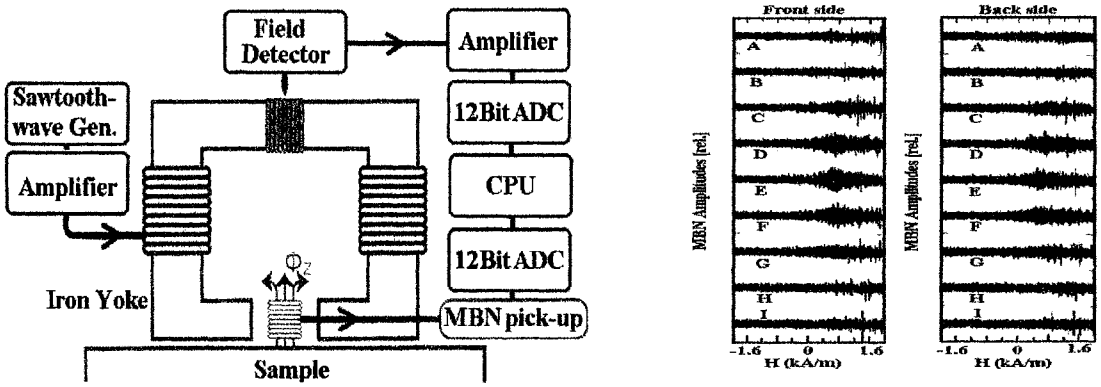

(a) (b-1) (b-2)

Fig.3 Experimental set-up of MBN observation and experimental results of MBN for SUS316

MBN was observed in a constant field sweep of 200kA/ms up to 16kA/m for a sample of S25C processed by shot-peening at one side of the sample at positions in between "C" and "G", where MBN were observed from a front side (b-1) of the shot-peening and backside (b-2), respectively. The positions "A","B",, ,"I" are illustrated in the sample on the plotter in Fig.1. Apparently, MBN were enhanced in the central positions in between "C"-"G" and observable even from backside of the sample.

Later on, experimental results for the other samples with large strains will be demonstrated together with leakage flux distributions for comparisons.

We performed observation of precise surface deformations with an accuracy of $\pm 3\,\mu$m by using a small unit system of CCD-Laser mounted at the pen-position in the plotter in Fig. 1. The inserted numbers in this figure denote the thickness deviations from the center (y=0).

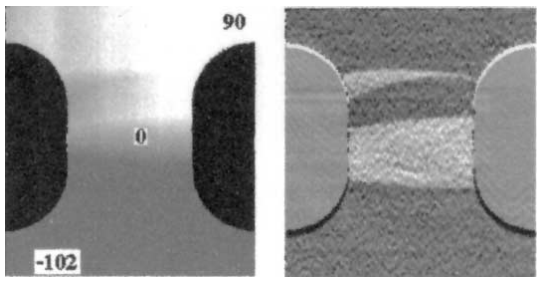

Fig.4 The thickness deformations D(x,y) and the derivative dD(x,y)/dx for S25C observed by a CCD-Laser device.
Note: In this figure, the relative thickness deviations at each position are colored by B&W as indicated by numbers in μm unit in the left figure.

In this stage of our experiments, we show the leakage flux distributions of S25C in Fig. 5 with several surface wrapping treatments to avoid lift-off distance changes by the surface deformations. The distribution patterns are almost similar with that in the surface deformations as in Fig. 4, reflecting the intrinsic effects of leakage flux distribution caused by material constant changes inside. These will be explained in the discussions.

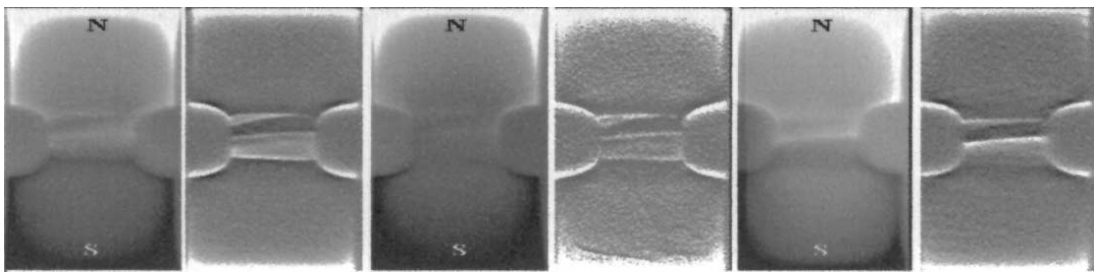

Fig. 5 The leakage flux observations for samples with several wrapping traetments
(a) The leakage flux distribution $B_Z^F(x,y)$ observed at the front side before surface wrapping,
(b) The first derivative $dB_Z^F(x,y)/dx$,(c) $B_Z^{FW}(x,y)$ after mechanical and chemical flat wrapping of 200 μm.
(d) $dB_Z^{FW}(x,y)/dx$,(e)$B_Z^B(x,d-y)$:the distribution observed from the back side. (f) $dB_Z^B(x,d-y)/dx$, respectively with the width d in y-direction

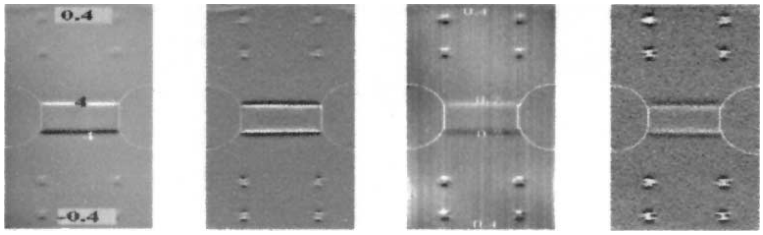

Fig. 6 The leakage flux distribution of a sample of SUS316 with peering one side surface observed from both sides
(a) The distribution $B_Z^F(x,y)$, (b) the first derivative $dB_Z^F(x,y)/dx$, (c) that from backside $B_Z^B(x,y)$ and (d) $dB_Z^B(x,y)/dx$

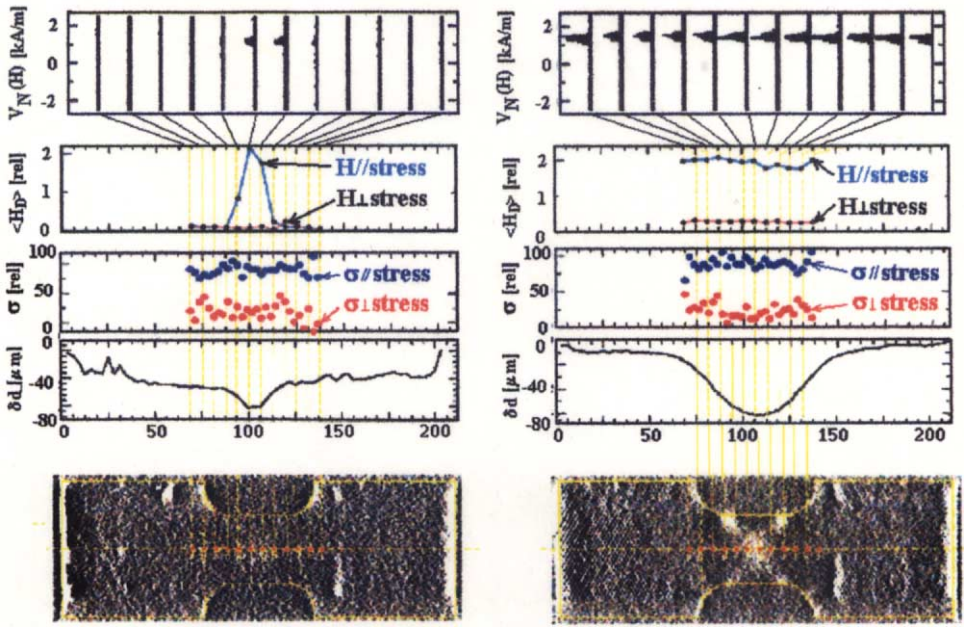

Fig.7 Comparisons of parameters together with leakage flux distributions for SUS304 samples with strains of 0.3 % (the left figure) and 4% (the right one), respectively

Fig. 6 (a)-(d) show the leakage flux distributions observed for SUS316 after shot-peening treatments at one surface side where the central parts show the step wise leakage flux enhancements denoted by the flux intensities of the leakage flux intensities in a unit of 10^{-4}T (=80A/m) for brevity. The flux distribution was observable even from backside.

Fig. 7 shows the experimental results of SUS304 samples with a slight strain and a heavy strain to compare all the parameters parallel with MBN, $<H_D>$, thickness deviations δd and the leakage flux as a function of positions. Here, $<H_D>$ was measured in different manners in parallel and perpendicular field configurations of magnetic yokes against the applied stresses along x direction. The differences between $<H_D>$*(H//stress)* and $<H_D>$*(H⊥stress)* suggests the anisotropy of the generated strains. The spatial dependence of $<H_D>$, residual stresses, thickness deformations are excellently coincided each other, except the original function of leakage flux distribution ($B_Z(x,y)$). The last one must be visualized by the first derivative as $dB_Z(x,y)/dx$, as mentioned before. Considering the nature of the leakage flux from a magnet, the inhomogeneity of the material constant is essential, which will be discussed later.

DISCUSSIONS

As we demonstrated in many figures and distribution patterns, the leakage flux distribution, its first derivative with respect to positions along the direction of applied stresses, MBN, $<H_D>$ and the other parameters are closely correlated each other. Now, in this section, we deduce the physical origins of these parameters.

First, the leakage flux $H(r)$ observed at r (outside of the magnet) or at x (1-D) are given by a magnetic potential $V_m(r)$ as

$$\mathbf{V}_m(\mathbf{r}) = \frac{1}{4\pi\mu_0}\iiint \frac{\rho(\mathbf{r}')(\mathbf{r}-\mathbf{r}')}{|\mathbf{r}-\mathbf{r}'|^3} d^3r' \qquad (1)$$

$$H(r) = -grad V_m(r) \quad , \qquad (2)$$

$$H_{1D}(x) = -\frac{1}{4\pi\mu_0} grad \int \frac{\rho(x')}{|x-x'|^2} dx' \quad . \tag{3}$$

Here, $\rho(r')$ denotes a microscopic local magnet moment at r', $B_{1D}(x)$, the observed flux density at x (outside of the magnet) for a one-dimensional magnet. The leakage flux intensity from a linear magnetic as expressed by Eq.(3), is informative to understand the leakage flux origin. Namely, the fluctuations of $H(x)$ is classified as follows. One is given by $\int \text{grad}\, \rho(x) \cdot 1/(x-x')^2 dx'$ and the other by $\int \rho(x) \cdot 1/(x-x')^3 dx'$. The former is given rise by the fluctuations of local moments that is essential in this investigation, and the second by the shape fluctuations. To discriminate the former term from the second one, the sample surface was wrapped flat mechanically, and etched chemically to take the surface off about 30μm. As shown in Fig. 5, the leakage flux distributions were unchanged for the different surfaces before and after the wrapping treatments, respectively. This fact suggests the leakage flux is dominantly generated by inhomogeneity of magnetic moments rather than the other parameters as the thickness variations in the present material and in these extents of deformations. These were simulated by using Eq.(1) and (2) as shown in Fig. 8. Here we used the experimentally obtained residual strains by XRD and thickness deformations at each point. In this simulation, the total magnetic energy composed of anisotropy energy and magnetostrictive energy was minimized to determine the orientations of local magnets.

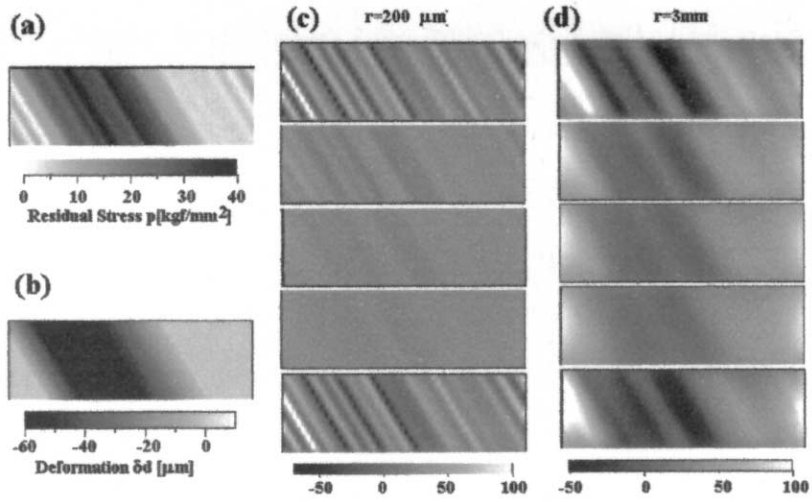

Fig.8 The simulations of the leakage flux observed at two different lift-off distances of (c) 0.2mm and (d) 3mm

Fig. 8 shows the results of simulations adopting the model as explained just before. Fig. 8(a) and (b) illustrate the distributions of residual stresses and thickness deformations colored in B&W. Fig.8(c) and (d) show the intensity of leakage flux density with a lift-off distance of 0.2 mm and 3 mm, respectively. As is easily noticed, the spatial resolution by using a small Hall element is almost determined by the lift-off distance as expected before hands.

Now, we discuss on the index $<H_D>$ derived by MBN. Usually the MBN amplitude varies with the touching manner of the pick-up coil at the surface. In this investigation, an index of the degradation $<H_D>$was defined by MBN signals as

$$< H_D(R,\theta) > \equiv \frac{\int_0^{t_{max}} H(t) V(R,\theta,h,t)\, dt}{\int_0^{t_{max}} V(R,\theta,h,t)\, dt} \tag{4}$$

$$\cong \frac{\int_0^{B_{max}} H_{int}\, dB_{int}}{\int_0^{B_{max}} dB_{int}} \tag{5}$$

Here, *H(t) and V(R, θ, h, t)* denote an applied magnetic field at time *t* and a BHN voltage in the pick-up coil at a position *R*, angle *θ* against the x direction, and a lift-off distance *h*, respectively. It is important to note here that the magnetic flux density B_{int}, H_{int} stand for the internal flux density and flux intensity, respectively, in contrast to *V(R, θ,h, t)* obtained outside of the material. Here we adopted a plausible approximation of Eq. (5) that observed leakage fluxes are connected by $dB_{int}/dt = C_L \cdot dB_{out}/dt = -V(R, \theta, h, t)$ appeared both in the nominator and the denominator in Eq. (4) [6,7]. By this reason, the quantity of $<H_D(R, \theta)>$ becomes insensitive against MBN amplitudes due to the common coefficient C_L in the nominator and denominator in Eq.(4). Equation (5) is now easily interpreted with the physical quantities inside [8,9,10,11,12] as

$$< H_D(R,\theta) >= \frac{1}{J} \sum_{j=0}^{J} \frac{\sum_{k=0}^{K_J} (x_{k,j} - x_{0,j}) \cdot H_k}{x_{Dj}} \tag{6}$$

Here, *J*, x_k stand for the total magnetic domain number inside of the detectable range for the mounted pick-up coil, the *k*'th domain jumping in a filed of H_k in the *j*'th magnetic domain. The physical quantity of $<H_D(R, \theta)>$ is now clarified that this parameter is monotonically proportional to the average field for the discontinuous magnetization if the continuous parts of the original MBN signals are subtracted. Fig.9 shows an example of $<H_D(R, \theta)>$ with an off-set of -60 kA/m as a function of angles measured from x-direction, at positions "F" (center) and "A" (sample corner) for a strained sample of 0.78%. It is apparent that Lüders band is tilted at 45 degrees caused by sheer stresses.

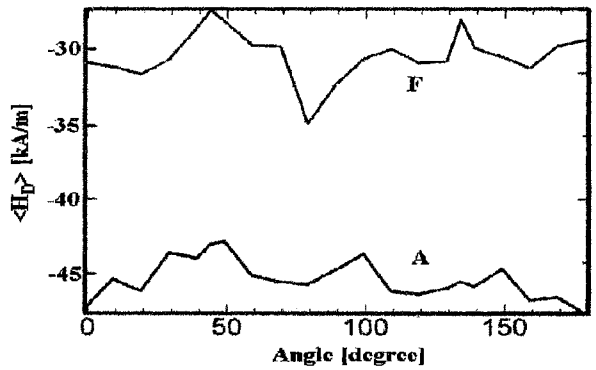

Fig 9 Average fields ($<H_D>$) for a strained sample of S25C

Experimentally, we obtained a linear relationship of $<H_D(R, \theta=0)>$ with the residual strain ε in a limited range of ε <3% for A533B as

$$<H_D(\theta=0)> \text{ [kA/m]} = 25 \pm 0.3 + (1.1 \pm 0.2)\ \varepsilon\ . \tag{7}$$

We found that the experimental values decreased and deviated from those given by Eq.(7) in a strain range between $4 < \varepsilon < 9$ and again increased in $10 < \varepsilon < 15$. Those behaviors are similar with the direct observations of ε by X-ray diffraction. It is worth while to note that $<H_D>$ varies with the sample thickness because applied fields (*H(t)* in Eq.(4), H_{int} in Eq.(5) and H_k in Eq. 6) must be effective fields inside of the sample, and these depend on the cross-section of the sample around the pick-up coil. Therefore, exactly speaking, Eq.(7) could not be determined from outside of the structure as a NDE tool. Finally, we show an investigation on the effects of material degradations on magnetizations by using a Monte-Carlo simulation of 50x50x50 spin arrays with a planar type spin voids. Because little investigation on magnetic behaviors had been done for NDE, we adopt a planar type lattice void as the first approach. Magnetizations with and without lattice imperfections were simulated as a function of temperatures with a physical model of RKKY [13,14,15] for spin interactions. Apparently, the magnetization decreased with increasing temperatures and decreased with the inclusion of a planar type lattice imperfection.

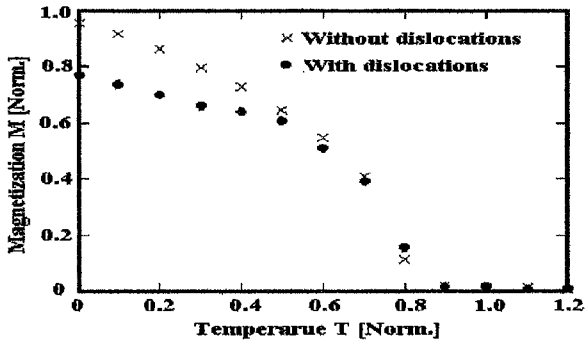

Fig. 10 Simulation of a magnetization as a function of ambient temperature with and without lattice dislocations

In this paper, however, NDE is the central point. By this reason, the leakage flux is visualized for these spin arrays with a lattice void plane in z-direction in an external field in z-direction. Fig. 11 shows the simulated leakage flux distribution if we can measure them with an enough spatial resolution. In this figure, blue and red colors denote incoming and out-going flux from the surface for z, y and x planes, respectively and the time elapses are numbered by 1 as the beginning stage of spin aligns and by 4 as the final saturation stage for each spin configuration plane of Sx, Sy and Sz, respectively. The role of a lattice void plane on the leakage flux distribution is clarified.

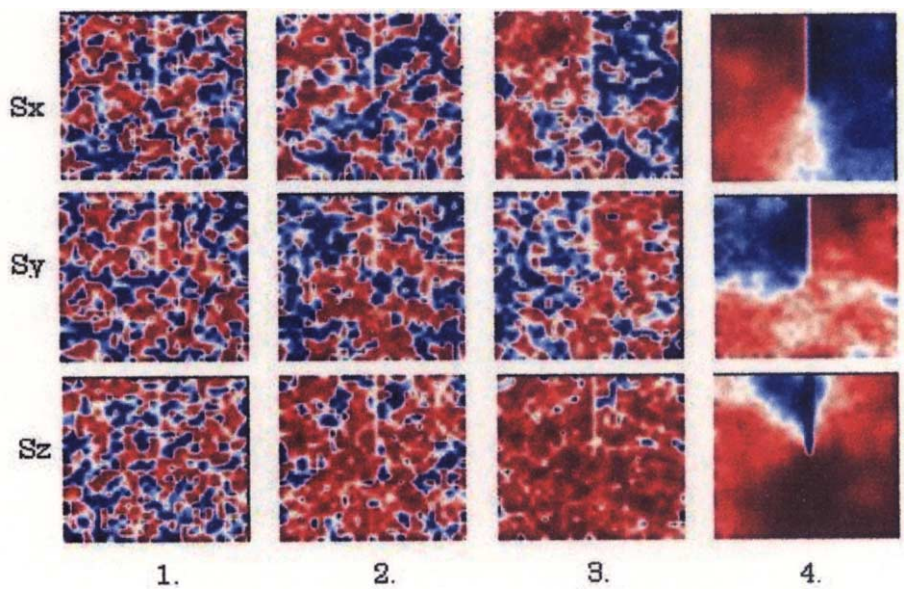

Fig.11 Simulated spin configurations for an applied field in z-direction

Further, it is plausible that in the saturation stage of spins (in the time step 4), the spin-up states (red) dominate over the plane due to the symmetry as depicted in Sz (4^{th} stage), and become polarized in spin-up at the left–half plane and spin-down (blue) as depicted in Sx and Sy (4^{th} stage), respectively. These pattern well explain and simulated the role of barriers by the atomic planar voids. The asymmetric spin configurations in Sy direction might be understood by the shear effect of the Lorenz force.

CONCLUSIONS

In this investigation, we succeeded in the visualizations of degradations via residual stress and magnetic domain distribution and/or leakage flux distribution. The MBN was processed by an index of $\langle H_D \rangle$, which shows a relationship with the residual

strains. The simulations for these leakage fluxes were well performed to help the understanding of the physical origins for the magnetic diagnosis.

Appendix.

Chemical compositions of the samples in Wt% and their preparation conditions

A533B (Fe, Mn_{18}, $Ni_{8,,,Mo,C,Si,Cu}$): ferromagnetic

Heat treatments: heating at 860-890C°for 2h25min-rapid quenching: annealing at 650-665C°for 2h19min-air cooling.

S25C (Fe, $Mn_{0.5}$, $C_{.0.24}$,$Si_{.0.24}$,$Cr_{.05,\ P,\ S,\ Cu,\ Ni,,}$): ferromagnetic,

Heat treatments: prescribed conditions.

SUS304 (Fe, Cr_{18}, $Ni_{8,,}$ $C_{0.08}$,Si_{1},Mn_{2},$P_{.0.45,,,}$): paramagnetic

Heating at 1050-1150cfor 1h - rapid quenching

SUS316 (Fe, Cr_{17}, $Ni_{10.6}$,$Mo_{2.19}$, $Mn_{1.03}$, $Si_{.0.68,,,}$):paramagnetic

Heating at 1050-1150C°for 1h .10min- rapid quenching.

REFERENCES

1. K. Yamada, S. Shoji, K. Yamaguchi and Y. Tanaka, "Fractal Dimension of Magnetic Noises :A Diagnosis Tool for Nondestructive Testing", Studies in Applied Electromagnetic and Mechanics No13, IOS Press Tokyo, ed. by Kose and J. Sievert, 1998, pp153-156
2. K. Yamada and T. Saitoh, "Observation of Barkhausen effect in ferromagnetic amorphous ribbon by sensitive pulsed magnetometer", J. Mag. Magn. Mater. Vol. 104,1991, p341-343
3. S. Ishige, Master Thesis (in Japanese), Saitama Univ., March 2000
4. S. Shoji, Doctor Thesis (in Japanese), Saitama Univ., March 1999
5. K. Yamada, S. Shoji, Y. Tanaka, Y. Uno, H. Takeda, M. Uesaka and K. Miya,, "Nondestructive Evaluation of Iron-based Material by Magnetic Sensor", Proc. of the "2nd Int. Workshop on Advanced Mechatronics" (IWAM'97), Nagasaki, 1997,pp114-119
6. K. Yamada, S. Shoji, Y. Tanaka, Y. Uno,H. Takeda, S. Toyooka, Spurapedi, Y. Isobe K. Ara, M. Uesaka and K. Miya., "Nondestructive Cross Evaluation of Iron-based Material by Magnetic Sensors and by Laser Speckle Interferometry", J. Magn. Soc. Jpn., 23, 1999,pp718-720
7. H. Kronmuler, Canadian J. Phys. Vol. 45(1967)
8. N. Hagiwara, N. Fukuda, T. Masuda and K. Yamada, "Nondestructive Evaluation of Plastic Strain in Pipeline Using Barkhausen Noises", Proc. Workshop on Magnetism and Lattice Imperfections, Hanamaki, Iwate, April, 2000, pp97-100
9. M. Uesaka, T. Sukegawa, K. Miya, S. Takahashi, J. Echigoya, K. Yamada, N. Kasai, K. Morishita, K. Ara, N. Ebine and Y. Isobe, "Round-robin test work for magnetic nondestructive evaluation of structural materials in nuclear power plants", Proc. Workshop on Magnetism and Lattice Imperfections, Hanamaki, Iwate, April, 2000,pp59-65
10. K. Yamada, K. Yamaguchi, S. Toyooka and Y. Isobe, 2magnetic and Optical Nondestructive Evaluation for Iron-based Materials", Nondestructive Characterization of Materials X, Ed. By R.E. Green et al., Elsevier Publ., Karuizawa, Japan, June 2000, p333-340
11. K. Yamaguchi, K. Yamada and Y. Isobe, "Monte-Carlo Simulation of Magnetization Processes including Lattice Imperfections", Proc. Int. Meeting on the relationship between Lattice Imperfection and Magnetism, Hanamaki, Iwate,April, 2000, pp69-71.
12. K. Yamada, K. Yamaguchi, H. Takeda, S. Tonooka, T. Masuda and N. Hagiwara, "Nondestructive cross evaluations iron-based material by optical and magnetic diagnosis tools", Invited paper for 3rd Int. Workshop on Advanced Mechatronic (IWAM'99), Chunchon, Korea, Dec. 1999, pp XXV-XXX
13. T. Kasuya, Prog. Theo. Phys. 16(1956)pp45-
14. K. Yoshida, Phys. Rev. 106(1957)pp893-
15. K. Yamaguchi, K. Yamada, "Simulation of Spin system for Nondestructive Evaluations of Iron-based Materials to be published by Proc. EMMA2000, May, Kiev 2000